Polarization Dynamics of Birefringent Index-guided Vertical Cavity Surface-Emitting Lasers

A. Valle[a], J. Martín–Regalado[b,c], L. Pesquera[a], S. Balle[c], and M. San Miguel[c]

[a] Instituto de Física de Cantabria (CSIC–UC), Facultad de Ciencias
Avda. Los Castros s/n, E–39005 Santander, Spain.

[b] Instituto Mediterráneo de Estudios Avanzados, IMEDEA (CSIC–UIB),
Universitat de les Illes Balears, E–07071 Palma de Mallorca, Spain.

[c] Departament de Física, Universitat de les Illes Balears, E–07071 Palma de Mallorca, Spain.

ABSTRACT

We study the polarization behavior of birefringent multi–transverse mode index–guided Vertical–Cavity Surface–Emitting Lasers (VCSELs) during CW and modulation operation. The model we use incorporates the α–factor, different carriers populations associated with different magnetic sublevels of the conduction and heavy hole valence bands in quantum well media, spin-flip relaxation processes and cavity anisotropies. The effect of carrier diffusion and spatial hole burning on the polarization behavior within the fundamental mode regime is also considered. We find that spin-flip dynamics and the α–factor are crucial for the selection of the polarization state corresponding to a given injection current. We also analyze the direct-current polarization modulation response for both the small and large signal modulation regimes. In both cases the current is modulated around the polarization switching (PS) current, but in the large signal modulation regime the current goes from below threshold to above the PS current. A frequency doubled polarized output is obtained under large signal modulation for modulation frequencies smaller than 10 MHz. At greater frequencies (around 100 MHz) transient mode polarization partition noise becomes important. At the greatest considered frequency (1 GHz) no PS is observed. Finally the effect of multiple transverse mode operation is addressed by considering the two lowest order modes: LP_{01} and LP_{11}.

Keywords: Vertical–cavity surface–emitting lasers, polarization switching, transverse modes, spin–flip relaxation, Spatial hole burning, birefringence, polarization modulation

1. INTRODUCTION

Due to the technological interest of Vertical–Cavity Surface–Emitting Lasers (VCSELs) considerable research effort has been devoted in recent years to understand their fundamental properties and, particularly, the polarization and transverse mode characteristics of these lasers.[1–21] The polarization behavior of VCSELs exhibit significant differences to those of conventional edge–emitting lasers where, typically, a well-defined linearly polarized state is retained for any current value. In VCSELs, light emitted is also linearly polarized but it can be oriented along one of two orthogonal crystal axes that are perpendicular to the emission direction. Hence, as the current is raised during fundamental mode operation it is possible to find either polarization stability,[1,2] polarization switching[3–8] or polarization coexistence.[1,4] For higher injection currents, changes in the emission profile linked to changes in the polarization state of the emitted light can also be observed after the onset of higher–order transverse modes, i.e., the first-order transverse mode usually starts lasing orthogonally polarized to the fundamental one.[4,7–10]

Several physical mechanisms have been proposed for the the selection of the polarization state. The first of these mechanisms is the thermally induced redshift of the polarized mode resonances relative to the gain peak.[4] The linearly polarized modes are frequency split — several GHz — due to the birefringence of the crystal.[10,11] As a consequence, they have slightly different material gains such that the polarized mode close to the gain-peak

Other author information: (Send correspondence to A.V.)
A.V.: Email: valle@soliton.unican.es; Telephone: 34-42-201465; Fax: 34-42-201459

dominates the emission. Within this framework, polarization switching should occur as the current is raised when the gain difference between the linearly polarized modes changes sign due to self–heating of the active region. However, this mechanism does not explain the polarization switching recently observed in gain–guided VCSELs when thermal effects are minimized by operating the laser with fast-pulse low-duty–cycle conditions.[12]

An alternative explanation to polarization state selection in VCSELs is the SFM model, which takes into account the combined effect of VCSEL anisotropies, the α factor and the spin-flip relaxation processes within a theoretical framework that includes the quantum states of the energy levels involved in the lasing process.[13] Such a framework is consistent with the experimental results in Ref. 12 and successfully describes the polarization characteristics of either VCSELs operating in the fundamental transverse mode[14,15] and of wide-area (gain-guided) multi-transverse mode devices.[16]

Finally, it has been shown that another mechanism that may cause polarization state selection in weak index-guided VCSELs is the combined effect of birefringency and spatial-hole burning, which causes differences in the modal gain of the waveguide transverse modes with orthogonal polarization.[17–21] The model used for these devices considers the dynamical evolution of the modal amplitudes of the built-in waveguide modes which are all coupled to the total carrier population through the modal profiles. In previous works, such a model has been extended to include spin-dynamics and the α-factor and has been applied to VCSELs operating in the fundamental transverse mode[15] showing that, for characteristic spin-flip relaxation rate values, spatial-hole burning effects have only a quantitative impact on the polarization effects attributed to spin-dynamics and the α-factor.

In this paper we study the polarization and transverse mode behavior of weak index-guided VCSELs that can operate in the fundamental, LP_{01}, and the first-order transverse mode, LP_{11}. We first study the polarization behavior of VCSELs that operate in the fundamental transverse mode. We review the steady state characteristics by showing polarization resolved L–I curves. We analyze the direct–current polarization modulation response for both the small and large signal modulation regimes. The multi–transverse mode regime is studied by showing polarization resolved L-I characteristics for the two lowest order transverse modes.

The paper is organized as follows. In Section 2 we extend the SFM model to incorporate spatial effects in index–guided multi–transverse mode VCSELs. Polarization modulation for VCSELs operating in the fundamental transverse mode is studied in Section 3. Polarization behavior of the fundamental and the first–order transverse modes is analyzed in Section 4. A summary of our results is given in Section 5.

2. MODEL FOR MULTI–TRANSVERSE MODE INDEX–GUIDED VCSELs

We consider cylindrically symmetric weak index-guided devices. Subscripts x and y will be used to denote the polarization direction. Birefringency is taken into account by assuming that the core refractive index in the $\hat{y}$ direction is smaller than in the $\hat{x}$ direction — hence the $\hat{x}$-polarized mode emission frequency is lower than that of the $\hat{y}$-polarized mode —, while the cladding refractive index is the same in both directions. We will consider small index steps Δn. Then the appropriate modes are the LP_{mn} modes.[22] Here we treat the case of VCSELs that can operate in the fundamental and in the first–order transverse modes. Subscripts $0,1$ will be used to denote the LP_{01} and the LP_{11} modes, respectively.

In the basis of the linearly polarized modes and considering the radial symmetry of the VCSEL cavity, the optical field can be written as

$$\mathbf{E}(r;t) = \left[\left(E_{0,x}(t)\psi_{0,x}(r) + E_{1,x}(t)\psi_{1,x}(r)\right)\mathbf{x} + \left(E_{0,y}(t)\psi_{0,y}(r) + E_{1,y}(t)\psi_{1,y}(r)\right)\mathbf{y}\right] e^{i\kappa\alpha t} + cc, \tag{1}$$

where $\psi_{0,i}$ and $\psi_{1,i}$ are the modal profiles of the LP_{01} and LP_{11} modes, respectively, obtained by solving the Helmholtz equation[17]; $E_{0,i}$ and $E_{1,i}$ are the modal amplitudes of these modes, and the subindex i stands for the linear polarization state of the given mode. The factor $e^{i\kappa\alpha t}$ takes into account a change in the frequency reference frame in such a way that the emission frequency is zero at threshold for perfectly isotropic devices. Hence, the equations describing the polarization behavior of the VCSEL, written appropriately in the cylindrical basis, read:

$$
\begin{aligned}
\dot{E}_{0,x} &= \kappa(1+i\alpha)[E_{0,x}(g_{0,x}-1)+iE_{0,y}\ g_{0,xy}] - (\gamma_a + i\gamma_{p,01})E_{0,x} \\
&+ \sqrt{\frac{\beta}{2}}\left[\sqrt{N+n}\ \xi_{\ 0,+}(t) + \sqrt{N-n}\ \xi_{\ 0,-}(t)\right] , \qquad (2) \\
\dot{E}_{0,y} &= \kappa(1+i\alpha)[E_{0,y}(g_{0,y}-1)-iE_{0,x}\ g_{0,yx}] + (\gamma_a + i\gamma_{p,01})E_{0,y} \\
&- i\sqrt{\frac{\beta}{2}}\left[\sqrt{N+n}\ \xi_{\ 0,+}(t) - \sqrt{N-n}\ \xi_{\ 0,-}(t)\right] , \qquad (3) \\
\dot{E}_{1,x} &= \kappa(1+i\alpha)[E_{1,x}(g_{1,x}-1)+iE_{1,y}\ g_{1,xy}] + i\gamma_p^{tr}E_{1,x} - (\gamma_a + i\gamma_{p,11})E_{1,x} \\
&+ \sqrt{\frac{\beta}{2}}\left[\sqrt{N+n}\ \xi_{\ 1,+}(t) + \sqrt{N-n}\ \xi_{\ 1,-}(t)\right] , \qquad (4) \\
\dot{E}_{1,y} &= \kappa(1+i\alpha)[E_{1,y}(g_{1,y}-1)-iE_{1,x}\ g_{1,yx}] + i\gamma_p^{tr}E_{1,y} + (\gamma_a + i\gamma_{p,11})E_{1,y} \\
&- i\sqrt{\frac{\beta}{2}}\left[\sqrt{N+n}\ \xi_{\ 1,+}(t) - \sqrt{N-n}\ \xi_{\ 1,-}(t)\right] , \qquad (5) \\
\partial_t N &= j(t)C(r) + \mathcal{D}\nabla_\perp^2 N \\
&- \gamma_e \left[N\left(1+\sum_{i=x,y}\ \sum_{j=0,1} |E_{j,i}|^2\psi_{j,i}^2\right) + in\sum_{j=0,1}\left(E_{j,x}E_{j,y}^* - E_{j,y}E_{j,x}^*\right)\psi_{j,x}\psi_{j,y}\right] , \qquad (6) \\
\partial_t n &= -\gamma_s n + \mathcal{D}\nabla_\perp^2 n \\
&- \gamma_e \left[n\left(\sum_{i=x,y}\ \sum_{j=0,1} |E_{j,i}|^2\psi_{j,i}^2\right) + iN\sum_{j=0,1}\left(E_{j,x}E_{j,y}^* - E_{j,y}E_{j,x}^*\right)\psi_{j,x}\psi_{j,y}\right] , \qquad (7)
\end{aligned}
$$

where $N(r,t)$ is the total carrier number and $n(r,t)$ is the difference in the carrier numbers of the two magnetic sublevels. $C(r)$ is the current density such that the total applied current is uniformly distributed across a circular disc contact of diameter $\phi = 6\ \mu m$, equal to the diameter of the active region, while the prefactor $j(t)$ allows for the generation of current ramps and for current modulation. The modal gain normalized to the threshold gain, $g_{j,i}(t)$ $(j=0,1;\ i=x,y)$, is defined as

$$
g_{j,i} = \frac{\int_0^\infty N(r;t)\psi_{j,i}^2(r)rdr}{\int_0^\infty \psi_{j,i}^2(r)rdr}, \qquad (8)
$$

and $g_{j,ik}(t)$ $(j=0,1;\ ik=xy,yx)$ is given by

$$
g_{j,ik}(t) = \frac{\int_0^\infty n(r,t)\psi_{j,i}(r)\psi_{j,k}(r)rdr}{\int_0^\infty \psi_{j,i}^2(r)rdr}. \qquad (9)
$$

The rest of the parameters that appear in the equations are: the field decay rate, κ=300 ns^{-1}; the linewidth enhancement factor, α=3; the decay rate of the total carrier population, γ_e=1 ns^{-1}; the decay rate of the carrier population difference through spin-flip relaxation processes,[23] γ_s; the diffusion constant, $\mathcal{D}$; the strength of their anisotropic gain/losses (dichroism), γ_a ; the frequency splitting between the fundamental, $\gamma_{p,01}$, and first-order, $\gamma_{p,11}$, transverse modes with orthogonal polarizations (birefringence); and the frequency splitting between the LP_{01} and LP_{11} transverse modes with the same polarization, γ_p^{tr}. The later three parameters are obtained from the calculation of the waveguide modes via the Helmholtz equation. Notice that we have considered a different birefringence for the LP_{01} and LP_{11} transverse modes, although the difference is typically negligible for weakly index-guided devices ($\gamma_{p,01} \sim \gamma_{p,11}$). A non vanishing value of γ_a can be due to the anisotropic gain of the crystal, the slightly different position of the frequency of the modes with respect to the gain versus frequency curve, and/or different cavity geometries for the differently polarized modes.

Spontaneous emission processes are modeled by the terms $\xi_\pm$ taken as complex Gaussian white noise sources of zero mean value and δ-correlated in time. In the noise terms, the carrier distribution is integrated over the active region of radius a:

$$\overline{N}(t) = \frac{\int_0^a N(r,t) r dr}{a^2} , \qquad \overline{n}(t) = \frac{\int_0^a n(r,t) r dr}{a^2} . \tag{10}$$

The equations of the model are numerically integrated via the discretization in space and time. Time and space integration steps of 0.01 ps and 0.12 μm, respectively, have been used. Different values of the spin–flip relaxation rate, and of the index step Δn are considered to study the combined effect of spin dynamics and spatial hole burning on the polarization properties of index–guided VCSELs. When Δn increases the difference between the optical transverse profiles for the $\hat{x}$ and $\hat{y}$ modes decreases, because the ratio of the birefringence to the index step increases. Then the modal gain anisotropy also decreases[18,19] and spatial hole burning effects have a smaller impact.

3. POLARIZATION BEHAVIOR OF THE FUNDAMENTAL TRANSVERSE MODE

In this section we study the polarization behavior of index–guided VCSELs that operate in the fundamental transverse mode. Several mechanisms of selection of this mode have been discussed in the literature[24,25] Previous studies have shown that the polarized light–current (L–I) characteristics are mainly determined by spin dynamics[15] for typical values of the spin–flip relaxation rate. Spatial effects only modify the location of the boundary between the different regions of the stability diagram obtained in the rate equation description.[14] However, when fast spin–flip relaxation rates ($\gamma_s > 200 \ \ \mathrm{ns}^{-1}$) are considered, polarization behavior can be determined by spatial hole burning effects.

3.1. Steady–state conditions

Prior to examining the modulation behavior, we review the steady state characteristics. We first consider the case without gain–loss anisotropy $\gamma_a = 0$ with a small birefringence $\gamma_{p,01} = 5.85 \ \ \mathrm{ns}^{-1} (\Delta\nu \sim 2$ GHz), $\mathcal{D} = 3$ cm^2/s, γ_s=50 ns^{-1}and $\Delta n = 0.005$. The inset of Fig. 1 shows the stability diagram of the linearly polarized solutions obtained without taking into account spatial effects. The $\hat{x}$–polarized mode is stable on the right and below the solid line. The $\hat{y}$–polarized mode is stable on the left of the dotted line. None of the linearly polarized modes are stable for large values of the birefringence when the injection current is increased. Just above threshold and for small values of the birefringence there is bistability of the two linearly polarized modes. However, when spatial effects are included in the description the $\hat{x}$–polarized mode is always selected at threshold. This selection is due to the modal gain anisotropy induced by birefringence. Since at low current values the carriers accumulate near the center of the active region, the modal gain of the better confined polarization, the $\hat{x}$–mode, is larger than that of the $\hat{y}$–mode (see Fig. 1). The polarized L–I characteristics shown in Fig.1 are obtained by increasing continuously the applied current, I, from 0.9 to 2 I_{th} during 200 ns, where $I_{th} = 0.3mA$ is the threshold current. The polarization switching $\hat{x} \to \hat{y}$ observed at $I \sim 1.45 I_{th}$ is due to the combined effect of the AM/FM coupling through the α-factor, VCSEL birefringence and spin dynamics,[14] since the $\hat{y}$–mode has less modal gain when is selected. However, the switching current is slightly higher than the one predicted by the rate equations approach due to spatial effects.

In order to force emission in the $\hat{y}$–polarization at threshold, we introduce an external gain–loss anisotropy favoring $\hat{y}$–polarization ($\gamma_a = 1 \ \ \mathrm{ns}^{-1}$). We also consider a higher birefringence $\gamma_p = 53 \ \ \mathrm{ns}^{-1}$(around 15 GHz), a higher spin–flip relaxation rate $\gamma_s = 100 \ \ \mathrm{ns}^{-1}$and an index step $\Delta n = 0.1$. This situation corresponds to the stability diagram shown in the inset of Fig. 2, which has been obtained by neglecting spatial effects. The $\hat{x}$ ($\hat{y}$)–polarized mode is stable on the right (left) of the solid (dotted) line. A polarization switching from the $\hat{y}$ to the $\hat{x}$ mode is expected when the injection current is increased. When spatial effects are considered this switching is delayed (see Fig. 2). This corresponds to the fact that the modal gain of the better confined $\hat{x}$–mode decreases when the injection current increases. The spatial hole burnt near the center of the active region in the

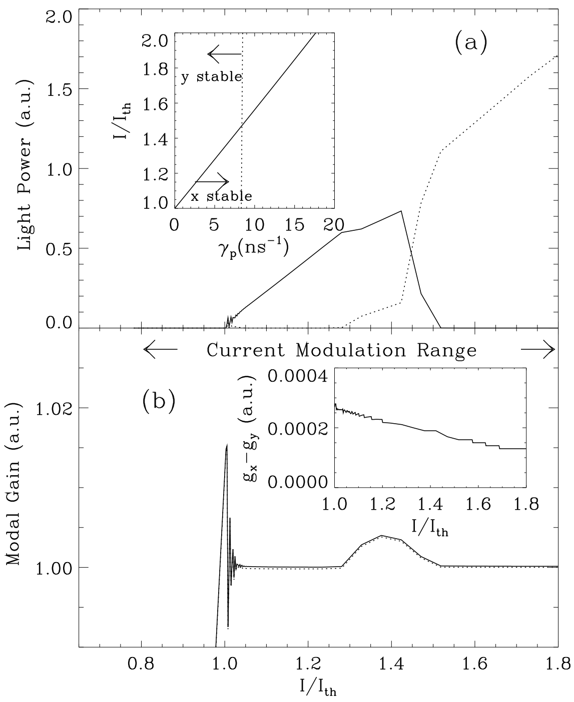

Figure 1. (a) L-I characteristic for the linear polarizations. The stability diagram appears in the inset. (b) Modal gain versus injection current. Curves related to the $\hat{x}(\hat{y})$ polarization are plotted with solid (dotted) lines. The inset shows the modal gain difference between the $\hat{x}$ and $\hat{y}$ polarizations.

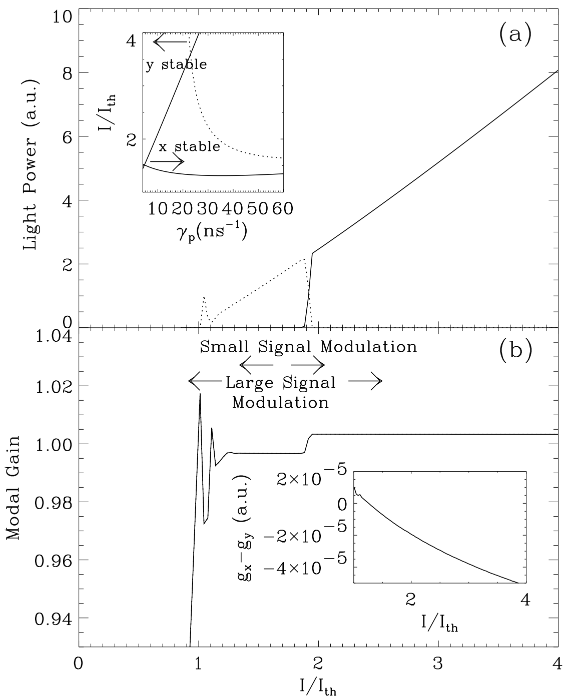

Figure 2. Same as Fig. 1 but for $\gamma_a = 1ns^{-1}, \gamma_p = 53ns^{-1}, \gamma_s = 100ns^{-1}$, and $\Delta n = 0.1$.

carrier profile is deeper, which leads to an accumulation of carriers towards the cladding region, and hence to a decrease in the modal gain of the better confined polarization. We remark that the $\hat{y} \rightarrow \hat{x}$ switching is observed even though the modal gain of the better confined $\hat{x}$–mode is smaller than that of the $\hat{y}$–mode due to spatial hole burning. This polarization switching is again due to the combined effect of spin dynamics, VCSEL anisotropies and the α-factor.

3.2. Modulation behavior

The polarization behavior of VCSELs can be exploited for modulation between the two linearly polarized modes. Polarization modulation at GHz frequencies has been accomplished through polarized optical feedback.[6,26–28] Polarization modulation has also been demonstrated by electrically driven the laser around its polarization switching current. Frequency doubling of the polarized output has been obtained for cruciform VCSELs[4,29] under large signal modulation for modulation frequencies smaller than 10 MHz. This behavior can not be explained by thermal effects. It has been shown that similar results are obtained for cylindrically symmetric weak index-guided devices by using a model that includes birefringence and spatial hole burning effects.[20]

In this section we incorporate in the description of Ref. 20 saturable dispersion associated with the α factor and the polarization–sensitive dynamics of the carriers. We explore the different behaviors that the polarization of a current modulated VCSEL can have. This analysis is performed for several values of the birefringence, dichroism, and frequency and amplitude of the modulation. We consider the response of the device to small and large signal modulation of the injected current around the polarization switching current. In the case of large signal modulation the current goes from below threshold to above the polarization switching current.

A sinusoidal modulation is considered for the injected current,

$$j(t) = j_b + j_m \sin(2\pi\nu_m t), \tag{11}$$

where j_b corresponds to a current close to the polarization switching current. We first study the case without external gain–loss anisotropy. When small signal modulation around the polarization switching current is considered, a modulated response polarized in the $\hat{y}$ direction is observed. This result is in agreement with the stability diagram shown in Fig. 1, since the $\hat{y}$–polarization is always stable in the range of low birefringences. However, under large signal modulation conditions at 1 MHz an out–of –phase response in both polarizations is obtained (see Fig. 3). In this case (j_b = 1.33 j_{th}, j_m = 0.5 j_{th}) the $\hat{x}$–polarization is selected when the laser switches on due to its higher modal gain. However, when the current decreases light emission is always polarized in the $\hat{y}$ direction.

When the $\hat{y}$–polarization is favored at threshold, a modulated response in both polarizations is obtained for small signal modulation. Fig. 4a shows the response of the device for j_b =1.67 J_{th}, j_m = 0.4 j_{th} and a modulation frequency of 1 MHz. When the injected current is decreasing a switching $\hat{x} \rightarrow \hat{y}$ is observed before $j(t)$ reaches its minimum value. Then the power of the $\hat{y}$–polarization decreases after the switching, before increasing with the injection current. However, for faster modulation frequencies (around 10 MHz) the power of the $\hat{y}$–polarization increases after this switching. The time the laser spends in the $\hat{y}$ polarization decreases when increasing the modulation frequency. This means that polarization switching mechanism is less effective as the modulation frequency is increased. In fact, when the modulation frequency is increased beyond 100 MHz no polarization switching is observed, and a modulated response polarized in the $\hat{x}$ direction is obtained.

The response of the laser to large signal modulation (j_b = 1.67 j_{th}, j_m = 0.8 j_{th}) at 1 MHz is shown in Fig. 4b. In this case two peaks of polarization mode $\hat{y}$ are obtained in each period of modulation. These two output peaks per input cycle arise from the cessation of lasing as the current goes below threshold, and from the switching to the $\hat{x}$–polarization as the current crosses the the polarization switching point. This behavior corresponds to that observed in Fig. 4a, but now the laser switches off when the current is below threshold. For greater modulation frequencies the small peak in the $\hat{y}$–polarization disappears, due to the delay in the response of the optical power to the changes in the injected current. When the modulation frequency is around 100 MHz fluctuations due to the spontaneous emission noise during laser switch–on become important (see Fig. 5). In this case the laser switches on in the polarization mode that is favored by the gain–loss anisotropy, $\hat{y}$. However, in some events the $\hat{x}$–polarization is selected at threshold and no polarization switching occurs during the modulation period. Finally, at frequencies around 1 GHz no polarization switching is observed.

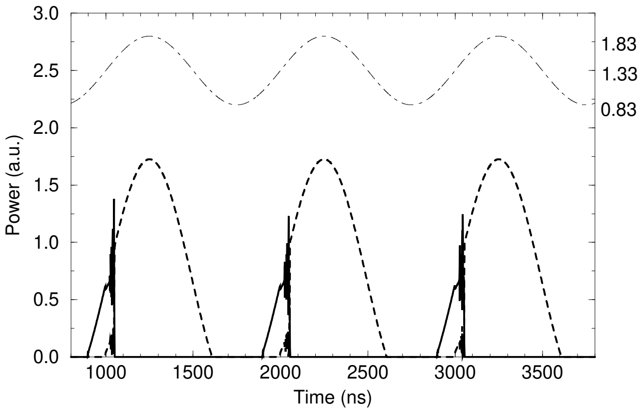

Figure 3. (a) Dynamic evolution of the linear polarizations power under current modulation. Curves related to the $\hat{x}(\hat{y})$ polarization are plotted as solid (dashed) lines. Applied current is also plotted with a dot–dashed line. Maximum, medium, and minimum current values (in threshold current units) are indicated at the right part. Parameters are as in Fig. 1.

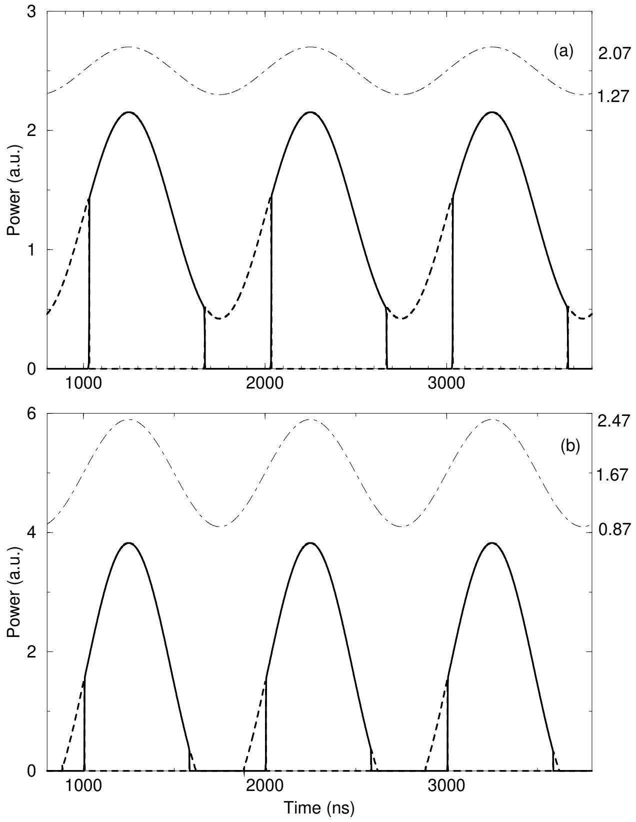

Figure 4. Dynamic evolution of the linear polarizations power under (a) small and (b) large signal modulation. Curves related to the $\hat{x}(\hat{y})$ polarization are plotted as solid (dashed) lines. Applied current is also plotted with dot–dashed lines. Maximum, medium, and minimum current values (in threshold current units) are indicated at the right part. Parameters are the corresponding to Fig. 2.

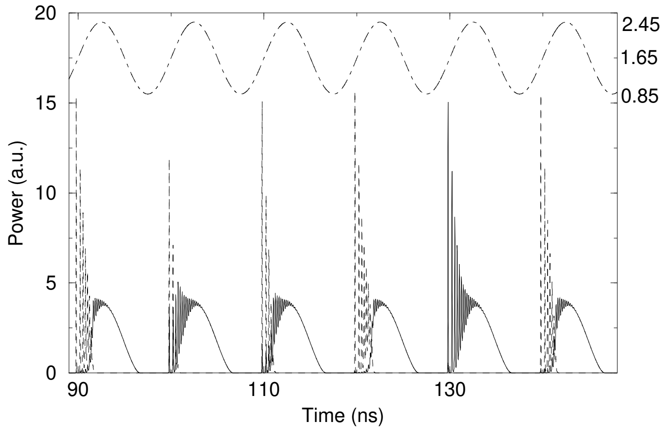

Figure 5. (a) Dynamic evolution of the linear polarizations power under 100 MHz current modulation. Curves related to the $\hat{x}(\hat{y})$ polarization are plotted as solid (dashed) lines. Applied current is also plotted with a dot–dashed line. Maximum, medium, and minimum current values (in threshold current units) are indicated at the right part. Parameters are the corresponding to Fig. 2.

4. POLARIZATION AND TRANSVERSE MODE BEHAVIOR OF MULTI-TRANSVERSE MODE VCSELs

In previous works[15,16] we numerically studied the polarization and transverse mode behavior of gain-guided VCSELs which can operate in several transverse modes corresponding to the same longitudinal mode. For this purpose, we used a generalized SFM model which included *(i)* transverse effects, such as optical diffraction and carrier diffusion; and *(ii)* the gain and dispersion spectra in a two-level Maxwell-Bloch approach. However, even though our results showed qualitative agreement with the experimental observations, it was not possible to identify completely the physical mechanisms governing the selection of the polarization state mediated by the transverse mode dynamics. For this reason, we explore in this section the polarization and transverse mode properties of weak index–guided VCSELs which can operate simultaneously in the fundamental and first–order transverse modes using the simpler model given by Eqs. (2)-(7). We have analyzed the possible Light-Current (L-I) characteristics in a variety of situations — different values of the dichroism, the birefringence and of the index step Δn have been considered to study the combined effect of spin dynamics and spatial-hole burning on the polarization properties of index-guided VCSELs — by increasing the applied current continuously from 0.95 to 3.5 I_{th} during the total simulation time (150 ns). In addition, the following values have been taken for the diffusion constant, $\mathcal{D}$ = 10 cm^2/s, and the spin–flip relaxation rate, γ_s=50 ns^{-1}, in all the simulations.

We first analyze the case of a very weak index-guided device (Δn = 0.005). Fig. 6(a) shows the L-I characteristics for a VCSEL with low birefringence ($\gamma_{p,01}$ = 3 ns^{-1}, $\Delta\nu = \gamma_{p,01}/\pi \sim$ 1 GHz) and vanishing dichroism (γ_a=0). The fundamental transverse mode starts lasing at threshold with $\hat{x}$-polarization since its modal gain is slightly larger than for the orthogonally polarized transverse mode (see Fig.6(b)). For increasing current, a polarization switching occurs at 1.2 I_{th} while the modal gain still favors the $\hat{x}$-polarized LP_{01} transverse mode. Such a switching is predicted in the SFM framework and is attributed to the AM-FM coupling through the α-factor.[14] For larger current values, emission occurs in the $\hat{y}$-polarized LP_{01} mode up to 2.1 I_{th}. At this current, an abrupt drop occurs in the total emitted power of the fundamental mode because of the onset of the LP_{11} mode. This mode starts lasing orthogonally polarized to the fundamental one in good agreement with previous experimental reports.[4,7–10] For even higher currents, the output power of the LP_{01} mode saturates and a polarization switching is observed but now between the LP_{11} modes with orthogonal polarizations.

We point out that such a behavior is the most likely one (36%) of the four possible L-I characteristics that can occur if the initial noise conditions are varied (the statistics is performed over 100 realizations). In a 31% of the realizations, $\hat{y}$-polarized stable emission during fundamental mode operation followed by an $\hat{x}$ to $\hat{y}$ polarization switching in the first-order transverse mode is observed. Stable emission in the $\hat{y}$-polarization occurs at any current value with a 20% of probability. Finally, in the 13% of the realizations, a polarization switching is observed during fundamental mode operation but stable $\hat{y}$-polarized LP_{11} emission occurs above 2.1

I_{th}. All these behaviors are consistent with the theory developed so far for single longitudinal and transverse mode VCSELs when the dichroism is zero.[14] Such a laser system is bistable close to the laser threshold and only the $\hat{y}$-polarized LP_{01} mode is stable above a certain switching threshold (see, i.e., the stability diagram in Fig. 1). Hence, the statistics show that the analysis developed for the fundamental mode can be also extended to the first-order transverse mode in order to explain the observed phenomena.

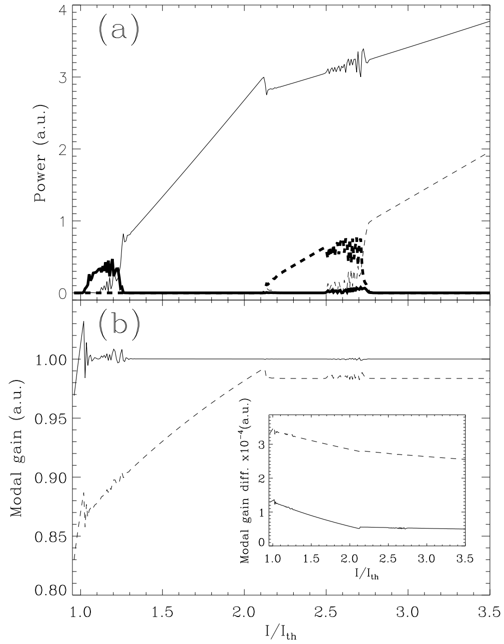

Figure 6. (a) L-I characteristics for a weak index-guided VCSEL with Δn=0.005, $\Delta\nu \sim 1$ GHz and γ_a=0: LP_{01} $\hat{x}$-polarized (solid bold), LP_{01} $\hat{y}$-polarized (solid), LP_{11} $\hat{x}$-polarized (dashed bold), LP_{11} $\hat{y}$-polarized (dashed). (b) Associated modal gain of the $\hat{x}$-polarized LP_{01} (solid) and LP_{11} (dashed) transverse modes. The inset shows the modal gain difference between the fundamental (solid) and first-order transverse modes with orthogonal polarizations.

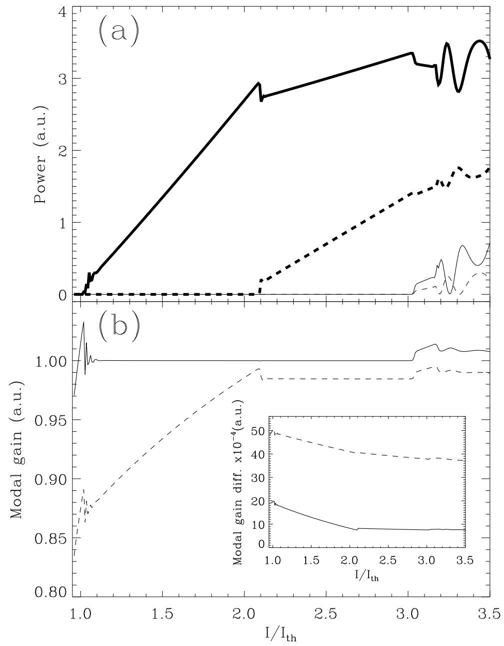

Figure 7. Same as Fig. 6 but for Δn=0.005, $\Delta\nu \sim 15$ GHz and γ_a=0.

The later statement is corroborated in Fig. 7 which corresponds to the same index-guided VCSEL but with a larger birefringence ($\Delta n = 0.005$, $\gamma_{p,01} = 45$ ns^{-1}, and γ_a=0). In this case the VCSEL emits in the $\hat{x}$-polarization at any value of the injected current, even after the onset of the first-order transverse mode. From the point of view of the theory developed so far,[14] this is the expected behavior in the range of large birefringences since the $\hat{y}$-polarized state is unstable in this regime (see, i.e., the stability diagram in Fig. 1). Nevertheless, such a L-I characteristics can be also attributed to the modal gain preference for the $\hat{x}$-polarization.

We finally analyze the case of a stronger index-guided VCSEL ($\Delta n = 0.01$) considering a more realistic gain anisotropy (γ_a=0.5 ns^{-1}) that favors the lower-wavelength ($\hat{y}$-polarized) LP_{01} mode at threshold. Fig. 8 shows the L-I characteristics for such a VCSEL when the birefringence is roughly 5 GHz. As a consequence of the amplitude anisotropy, emission starts in the $\hat{y}$-polarized LP_{01} mode but, for increasing current, a polarization switching to the $\hat{x}$-polarized fundamental mode appears at 1.3 I_{th}. Such a switching corresponds to the one observed in a recent experiment performed under similar fast-current-ramp conditions[12] and it is due to the combined effect of spin-dynamics, the α-factor and VCSEL anisotropies.[14] At 1.5 I_{th}, VCSEL emission goes into the multi-transverse mode regime where simultaneous emission of the $\hat{x}$-polarized LP_{01} and the $\hat{y}$-polarized LP_{11} transverse modes remains for the rest of the current range investigated. Such a polarization and transverse mode behavior is still observed for similar but higher birefringence VCSELs, the only difference being the appearance of an additional abrupt $\hat{y}$ to $\hat{x}$ polarization switching between the LP_{11} transverse modes in the L-I characteristics.

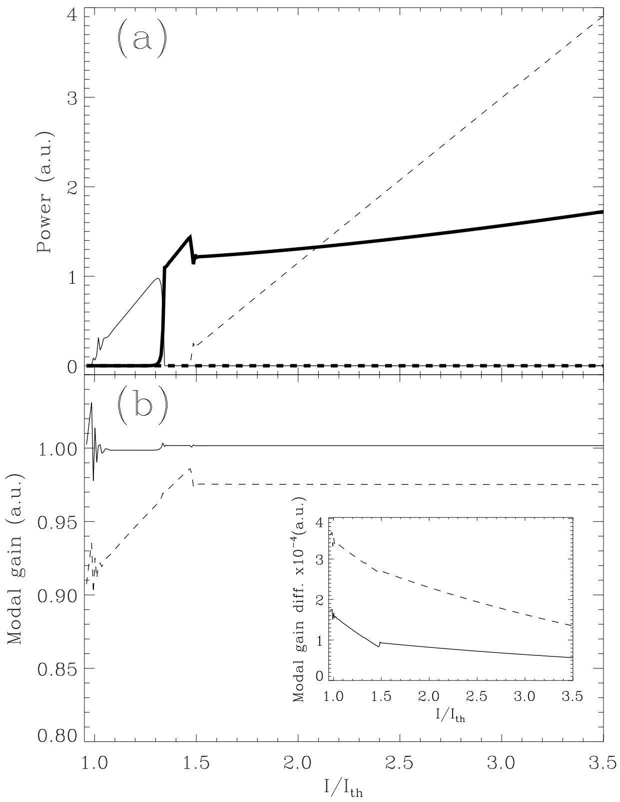

Figure 8. Same as Fig. 6 but for Δn=0.01, $\Delta\nu \sim 5$ GHz and γ_a=0.5 ns^{-1}.

5. SUMMARY AND CONCLUSSIONS

The polarization behavior of birefringent multi–transverse mode index–guided VCSELs during CW and modulation operation has been analyzed. We have found that spin-flip dynamics, VCSEL anisotropies and the α–factor are relevant mechanisms for the selection of the polarization state corresponding to a given injection current, although the influence of spatial-hole burning and thermal effects should be also considered. Regarding the modulation properties of these lasers, a frequency doubled polarized output has been obtained under large signal modulation for modulation frequencies smaller than 10 MHz. At greater frequencies (around 100 MHz) we have shown that transient mode polarization partition noise becomes important. For higher frequencies (around 1 GHz) no polarization switching was observed. Finally, the effect of multiple transverse mode operation has been addressed, and we have shown that the physical mechanisms governing the selection of the polarization state for the fundamental mode are the same than for the first-order transverse mode.

6. ACKNOWLEDGEMENTS

We acknowledge financial support from CICYT (Spain) projects TIC95/0563 and PB94–1167, European Union project UFMRX-CT96-0077, and Caja Cantabria.

REFERENCES

1. K. D. Choquette and R. E. Leibenguth, "Control of vertical-cavity laser polarization with anisotropic transverse cavity geometries", *IEEE Photon. Technol. Lett.* **6**, pp. 40–42 (1994).
2. F. Koyama, K. Morito, and K. Iga, "Intensity noise and polarization stability of GaAlAs–GaAs surface emitting lasers", *IEEE J. Quantum Electron.* **27**, pp. 1410–1416 (1991).
3. H. Li, T. L. Lucas, J. G. McInerney and R. A. Morgan, "Transverse modes and patterns of electrically pumped vertical-cavity surface-emitting semiconductor lasers", *Chaos, Solitons and Fractals* **4**, pp. 1619–1636 (1994).
4. K. D. Choquette, D. A. Richie, and R. E. Leibenguth, "Temperature dependence of gain-guided vertical-cavity surface emitting laser polarization", *Appl. Phys. Lett.* **64**, pp. 2062–2064 (1994).
5. Z.G. Pan, S. Jiang and M. Dagenais, R.A. Morgan, K. Kojima, "Optical injection induced polarization bistability in vertical-cavity surface-emitting lasers", M.T. Asom, R.E. Leibenguth, G.D. Guth, and M.W. Focht, *Appl. Phys. Lett.* **63**, pp. 2999–3001 (1993).
6. S. Jiang, Z. Pan, M. Dagenais, R. A. Morgan and K. Kojima, "High-frequency polarization self-modulation in vertical-cavity surface-emitting lasers", *Appl. Phys. Lett.* **63**, pp. 3545–3547 (1993).
7. K. D. Choquette, R. P. Schneider, Jr., K. L. Lear, and R. E. Leibenguth, "Gain-dependent polarization properties of Vertical-Cavity lasers", *IEEE J. Select. Topics Quantum Electron.* **1**, pp. 661–666 (1995).
8. J. H. Ser, Y. G. Ju, J. H. Shin, and Y. H. Lee, "Polarization stabilization of vertical-cavity surface emitting lasers by inscription of fine metal-interlaced gratings", *Appl. Phys. Lett.* **66**, pp. 2769–2771 (1995).
9. U. Fiedler, G. Reiner, P. Schnitzer, and K. J. Ebeling, "Top surface-emitting vertical-cavity laser diodes for 10-Gb/s data transmission", *IEEE Photon. Technol. Lett.* **8**, pp. 746–748 (1996).
10. M. P. van Exter, A. K. Jansen van Doorn, and J. P. Woerdman, "Transverse anisotropy and mode structure in VCSELs", in *Physics and Simulation of Optoelectronic Devices IV*, SPIE Vol. **2693**, 202 (1996).
11. A. K. Jansen van Doorn, M. P. van Exter and J. P. Woerdman, "Effects of transverse anisotropy on VCSEL spectra", *Electron. Lett.* **30**, 1941 (1994); *Phys. Rev. A* **56**, 845 (1997).
12. J. Martín-Regalado, J. L. A. Chilla, J. J. Rocca, and P. Brusenbach, "Polarization Switching in Vertical-Cavity Surface Emitting Lasers observed at Constant Active Region Temperature", *Appl. Phys. Lett.* **70**, pp. 3350–3352 (1997).
13. M. San Miguel, Q. Feng, J. V. Moloney, "Light-polarization dynamics in surface-emitting semiconductor lasers", *Phys. Rev. A* **52**, pp. 1728–1739 (1995).
14. J. Martín-Regalado, M. San Miguel, N. B. Abraham, F. Prati, "Polarization Switching in Quantum Well Vertical-Cavity Surface Emitting Lasers", *Opt. Lett.* **21**, pp. 351–353 (1996); "Polarization Properties of Vertical Cavity Surface Emitting Lasers", *IEEE J. Quantum Electron.*, **33**, pp. 765–783 (1997).
15. J. Martín-Regalado, S. Balle, M. San Miguel, A. Valle and L. Pesquera, " Polarization and transverse mode selection in quantum well vertical–cavity surface emitting lasers: index and gain guided devices", *Quantum and Semiclass. Opt.* **9**, pp. 713–736 (1997).
16. J. Martín-Regalado, S. Balle, and M. San Miguel, "Polarization and transverse mode dynamics of gain-guided vertical-cavity surface emitting lasers", *Optics Lett.* **22**(7), pp. 460–462 (1997).
17. A. Valle, K. A. Shore, and L. Pesquera, "Polarization selection in birefringent vertical cavity surface emitting lasers", *IEEE J. of Lightwave Tech.* **14**, pp. 2062–2068 (1996).

18. A. Valle, L. Pesquera, and K. A. Shore, "Polarization behavior of birefringent multi-transverse mode Vertical-Cavity Surface Emitting Lasers", *IEEE Photon. Technol. Lett.* **9**, pp. 557–559 (1997).
19. A. Valle, L. Pesquera, and K. A. Shore, "Polarization and transverse mode selection in birefringent Vertical-Cavity Surface Emitting Lasers", in *Physics and Simulation of Optoelectronic Devices V*, SPIE Vol. **2994**, pp. 168–176 (1997).
20. A. Valle, L. Pesquera, and K. A. Shore, "Polarization modulation dynamics of birefringent vertical-cavity surface-emitting lasers", *IEE Proc. Optoelectron.* (1998).
21. R. Mueller, A.Khler, A. Valle, J. Sarma, and K. A. Shore, "Effects of Spatial Hole-Burning effects on polarization dynamics in edge-emitting and vertical cavity surface emitting laser diodes", *Semiconductor Science and Technology* **11**, pp. 587–596 (1996).
22. A. Valle, J. Sarma, and A. Shore, "Spatial Hole Burning Effects on the dynamics of Vertical Cavity Surface Emitting Laser Diodes", *IEEE J. Quantum Electron.*, **31**, pp. 1423–1431 (1995).
23. L. J. Sham, "Spin relaxation in semiconductor quantum wells", *J. Phys. Condens. Matter* **5**, A51 pp. 51–60 (1993).
24. R. A. Morgan, G. D. Guth, M. W. Focht, M. T. Asom, L. E. Rogers, and S. E. Callis, "Transverse mode control of vertical-cavity top-surface emitting lasers", *IEEE Phot. Tech. Lett.* **4**, pp. 374–376 (1993).
25. M. Ogura, S. Fuiji, T. Okada, M. Mori, K. Mori, T. Asaka, and H. Iwano, "Transverse mode characteristics of a DBR surface emitting laser with buried heterostructure", *Jap. J. of Appl. Physics* **30**, No. 12B, pp. 3879–3882 (1991).
26. F. Robert, P. Besnard, M-L. Chares, and G. M. Stephan, "Switching of the polarization state of a vertical–cavity surface–emitting laser using polarized feedback", *Optical and Quantum Electron.*, **27**, pp. 805–811 (1995).
27. P. Besnard, F. Robert, M-L. Chares, and G. M. Stephan, "Theoretical modeling of vertical–cavity surface–emitting laser with polarized optical feedback", *Physical Review A*, **56**, pp. 3191–3205 (1997).
28. F. Robert, P. Besnard, M-L. Chares, and G. M. Stephan, "Polarization modulation dynamics of vertical–cavity surface–emitting lasers with an extended cavity", *IEEE J. Quantum Electron.*, **33**, pp. 2231–2239 (1997).
29. K. D. Choquette, K. L. Lear, R. P. Schneider, Jr., R. E. Leibenguth, J. J. Figiel, S. P. Kilcoyne, M. Hagerott-Crawford, and J. C. Zolper, "Polarization characteristics, control, and modulation of vertical-cavity surface emitting lasers", in *Laser Diodes and Applications*, K. J. Linden and P. R. Akkapeddi, eds., **2382** 125, (SPIE, Bellingham, 1995).